# Appendix A

# TASOPT — Transport Aircraft System OPTimization

## A.1 Introduction

### A.1.1 Background

There is a vast body of work on conceptual and preliminary aircraft design. The more traditional approaches of e.g. Roskam [1], Torrenbeek [2], Raymer [3], have relied heavily on historical weight correlations, empirical drag build-ups, and established engine performance data for their design evaluations. The ACSYNT program [4],[5] likewise relies on such models, with a more detailed treatment of the geometry via its PDCYL [6] extension.

More recently, optimization-based approaches such as those of Knapp [7], the WINGOP code of Wakayama [8],[9], and in particular the PASS program of Kroo [10] perform tradeoffs in a much more detailed geometry parameter space, but still rely on simple drag and engine performance models.

The recent advent of turbofan engines with extremely high bypass ratios (Pratt geared turbofan), advanced composite materials (Boeing 787), and possibly less restrictive operational restrictions (Free-Flight ATC concept), make it of great interest to re-examine the overall aircraft/engine/operation system to maximize transportation efficiency. NASA's N+1,2,3 programs are examples of research efforts towards this goal. In addition, greater emphasis on limiting noise and emissions demands that such aircraft design examination be done under possibly stringent environmental constraints. Optimally exploiting these new factors and constraints on transport aircraft is a major motivation behind TASOPT's development.

### A.1.2 Summary

#### Overall approach

To examine and evaluate future aircraft with potentially unprecedented airframe, engine, or operation parameters, it is desirable to dispense with as many of the historically-based

methods as possible, since these cannot be relied on outside of their data-fit ranges. The approach used by TASOPT is to base most of the weight, aerodynamic, and engine-performance prediction on low-order models which implement fundamental structural, aerodynamic, and thermodynamic theory and associated computational methods. Historical correlations will be used only where absolutely necessary, and in particular only for some of the secondary structure and for aircraft equipment. Modeling the bulk of the aircraft structure, aerodynamics, and propulsion by fundamentals gives considerable confidence that the resulting optimized design is realizable, and not some artifact of inappropriate extrapolated data fits.

### Airframe structure and weight

The airframe structural and weight models used by TASOPT treat the primary structure elements as simple geometric shapes, with appropriate load distributions imposed at critical loading cases. The fuselage is assumed to be a pressure vessel with one or more "bubbles", with added bending loads, with material gauges sized to obtain a specified stress at specified load situations. The wing is assumed to be cantilevered or to have a single support strut, whose material gauges are also sized to obtain a specified stress. The resulting fuselage, wing, and tail material volumes, together with specified material density, then gives the primary structural weight. Only the secondary structural weights and non-structural and equipment weights are estimated via historical weight fractions.

### Aerodynamic performance

The wing airfoil performance is represented by a parameterized transonic airfoil family spanning a range of thicknesses, whose performance is determined by 2D viscous/inviscid CFD calculation for a range of lift coefficients and Mach numbers. Together with suitable sweep corrections, this gives reliable profile+wave drag of the wing in cruise and high climb and high descent. The fuselage drag is likewise obtained from compressible viscous/inviscid CFD, suitably simplified with axisymmetric-based approximations. A side benefit is that detailed knowledge of the fuselage boundary layers makes it possibly for TASOPT to reliably predict the benefits of boundary layer ingestion in fuselage-mounted engines.

The drag of only the minor remaining components such as nacelles is obtained by traditional wetted area methods, but corrected for supervelocities estimated with vortex sheet models. Induced drag is predicted by fairly standard Trefftz-Plane analysis.

The primary use of CFD-level results in the present TASOPT method makes it more widely applicable than the previous more traditional approaches which have typically relied on wetted-area methods for major components of the configuration.

### Engine performance

A fairly detailed component-based turbofan model, such as described by Kerrebrock [11], is used to both size the engines for cruise, and to determine their off-design performance at takeoff, climb, and descent. The model includes the effects of turbine cooling flows, allowing realistic simultaneous optimization of cycle pressure ratios and operating temperatures

together with the overall airframe and its operating parameters. The overall aircraft and engine system is actually formulated in terms of dissipation and power rather than drag and thrust [12], which allows a rigorous examination of advanced propulsion systems using boundary layer ingestion.

The use of component-based engine simulation in the present TASOPT method differs from previous approaches which typically have relied on simple historical regressions or established engine performance maps. The more detailed treatment is especially important for examining designs with extreme engines parameters which fall outside of historical databases.

#### Mission profiles

Integration of standard trajectory equations over a parameterized mission profile provides the required mission weight, which completes the overall sizing approach. The end result is a defined aircraft and engine combination which achieves the specified payload and range mission. Off-design missions are also addressed, allowing the possibility of minimizing fuel burn for a collection of fleet missions rather than for just the aircraft-sizing mission.

#### Takeoff and noise

A takeoff performance model is used to determine the normal takeoff distance and the balanced field length of any given design. The balanced field length can be included as a constraint in overall TASOPT optimization. Noise estimates are also calculated using a few published methods, e.g. [13], [14], [15]. These are used only for run-time rough estimates, and are not well suited for use as constraints. Much more detailed noise analyses can typically be performed as a post-processing step using the ANOPP method, for example.

#### Restriction to wing+tube aircraft

The description of the structural and aerodynamic models above explains why TASOPT is restricted to tube+wing configurations — most other configurations would be quite difficult or impossible to treat with these models. For example, a joined-wing configuration [16] has a relatively complex structure with out-of-plane deformations and the possibility of coupled twist/bend buckling in the presence of eccentricity from the airloads, which requires a greatly more complex structural analysis than straightforward beam theory. A blended-wing-body configuration [17] with non-circular cabin cross sections likewise has non-obvious critical load cases and load paths, and its transonic aerodynamics are dominated by 3D effects. For these reasons such non-traditional configurations are simply outside the scope of the present work.

## A.2 Model Derivation

### A.2.1 Weight Breakdown

The weight breakdown is summarized in Figure A.1, to serve as a convenient reference.

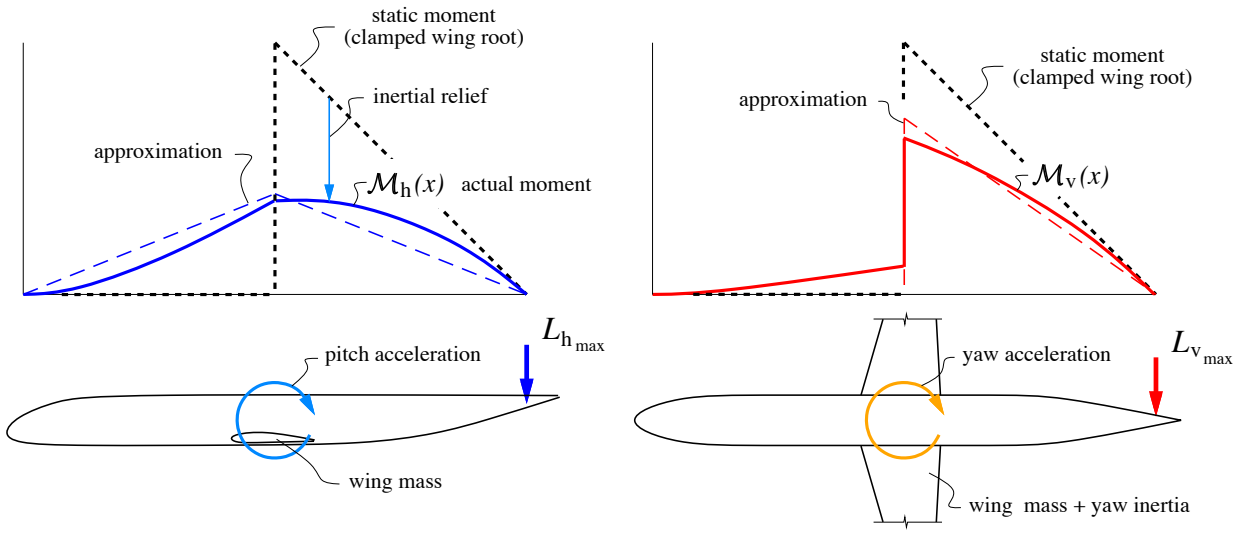


Figure A.5: Fuselage bending moments due to unbalanced horizontal and vertical tail aero loads. The static bending moment (dashed lines) is partly relieved by reaction loads from the overall angular acceleration.

### Distributed and point weight loads

The fuselage is loaded by the payload weight $W_{\text{pay}}$, plus its own component weights $W_{\text{padd}}$, $W_{\text{shell}}$ ... etc. which are all assumed to be uniformly distributed over the fuselage shell length $l_{\text{shell}}$. The overall tail weight $W_{\text{tail}}$ is assumed to be a point load at $x_{\text{tail}}$. With all weights scaled up by a load factor $N$, plus the impulsive horizontal-tail aero load moment (A.74), gives the following quadratic+linear horizontal-axis fuselage bending moment distribution, also sketched in Figure A.2.

$$\begin{aligned}\mathcal{M}_{h(x)} &= N\,\frac{W_{\text{pay}}+W_{\text{padd}}+W_{\text{shell}}+W_{\text{window}}+W_{\text{insul}}+W_{\text{floor}}+W_{\text{seat}}}{2\,l_{\text{shell}}}\,(x_{\text{shell}\,2}-x)^2 \\ &+ \;(NW_{\text{tail}}+r_{\text{Mh}}L_h)\,(x_{\text{tail}}-x)\end{aligned} \tag{A.79}$$

Expression (A.79) has been constructed to represent the bending moment over the rear fuselage. Since the wing's inertial-reaction pitching moments are small compared to those of the tail and fuselage, the horizontal-axis bending moment is assumed to be roughly symmetric about the wing's center of lift at $x_{\text{wing}}$, as sketched in Figure A.2, so that (A.79) if reflected about $x_{\text{wing}}$ also gives the bending moment over the front fuselage. For the same reason, the fixed weight $W_{\text{fix}}$ is assumed to be concentrated near the aircraft nose, and hence it does not impose either a distributed load or a point load on the rear fuselage, and hence does not appear in (A.79).

### Added horizontal-axis bending material

The total bending moment $\mathcal{M}_{h(x)}$ defined by (A.79) is used to size the added horizontal-axis bending area $A_{\text{hbend}(x)}$. Two loading scenarios are considered:

1. Maximum load factor at $V_{NE}$

$$N = N_{\text{lift}} \tag{A.80}$$
$$L_{\text{h}} = L_{\text{h}_{\max}} \tag{A.81}$$

2. Emergency landing impact

$$N = N_{\text{land}} \tag{A.82}$$
$$L_{\text{h}} = 0 \tag{A.83}$$

The scenario which gives the larger added structural weight will be selected.

The maximum axial stress, which is related to the sum of the bending and pressurization strains, is limited everywhere to some maximum allowable value $\sigma_{\text{bend}}$.

$$E_{\text{bend}}\epsilon_{x(x)} = E_{\text{bend}}\left(\epsilon_{\text{bend}(x)} + \epsilon_{\text{press}}\right) \leq \sigma_{\text{bend}} \tag{A.84}$$
$$r_E\left(\frac{\mathcal{M}_{\text{h}(x)}\, h_{\text{fuse}}}{I_{\text{hshell}} + r_E\, I_{\text{hbend}(x)}} + \frac{\Delta p}{2}\frac{R_{\text{fuse}}}{t_{\text{shell}}}\right) \leq \sigma_{\text{bend}} \tag{A.85}$$
$$\text{where} \qquad h_{\text{fuse}} = R_{\text{fuse}} + \tfrac{1}{2}\Delta R_{\text{fuse}} \tag{A.86}$$

Relation (A.85) can then be solved for the required $I_{\text{hbend}(x)}$ and the associated $A_{\text{hbend}(x)}$.

$$I_{\text{hbend}(x)} = \max\left(\frac{\mathcal{M}_{(x)}\, h_{\text{fuse}}}{\sigma_{\text{Mh}}} - \frac{I_{\text{hshell}}}{r_E}\ ,\ 0\right) \tag{A.87}$$
$$\text{where} \qquad \sigma_{\text{Mh}} = \sigma_{\text{bend}} - r_E\frac{\Delta p}{2}\frac{R_{\text{fuse}}}{t_{\text{shell}}} \tag{A.88}$$
$$A_{\text{hbend}(x)} = \frac{I_{\text{hbend}(x)}}{h_{\text{fuse}}^2} = A_2(x_{\text{shell}\,2} - x)^2 + A_1(x_{\text{tail}} - x) + A_0 \tag{A.89}$$
$$\text{where} \qquad A_2 = \frac{N(W_{\text{pay}} + W_{\text{padd}} + W_{\text{shell}} + W_{\text{window}} + W_{\text{insul}} + W_{\text{floor}} + W_{\text{seat}})}{2\, l_{\text{shell}}\, h_{\text{fuse}}\, \sigma_{\text{Mh}}} \tag{A.90}$$
$$A_1 = \frac{NW_{\text{tail}} + r_{\text{Mh}}L_{\text{h}}}{h_{\text{fuse}}\, \sigma_{\text{Mh}}} \tag{A.91}$$
$$A_0 = -\frac{I_{\text{hshell}}}{r_E\, h_{\text{fuse}}^2} \tag{A.92}$$

The volume and weight of the added bending material is defined by integration of $A_{\text{hbend}}$, from the wing box to the location $x = x_{\text{hbend}}$ where $A_{\text{hbend}} = 0$ in the quadratic definition (A.89). If this quadratic has no real solution, then the inequality (A.79) holds for $\mathcal{M}_{\text{h}(x)} = 0$ everywhere, and no added bending material is needed.

Two separate integration limits are used for the front and back fuselage, to account for the shifted wing box for a swept wing. The integral for $\mathcal{V}_{\text{hbend}_f}$ for the front fuselage is actually computed over the back, by exploiting the assumed symmetry of $\mathcal{M}_{\text{h}(x)}$ and $A_{\text{hbend}(x)}$ about $x = x_{\text{wing}}$. The wing box offset $\Delta x_{\text{wing}}$ is computed later in the wing-sizing section, so here it is taken from the previous iteration.

$$x_f = x_{\text{wing}} + \Delta x_{\text{wing}} + \tfrac{1}{2}c_o\bar{w} \tag{A.93}$$

$$
\begin{aligned}
x_b &= x_{\text{wing}} - \Delta x_{\text{wing}} + \tfrac{1}{2} c_o \bar{w} && \text{(A.94)} \\
\mathcal{V}_{\text{hbend}_f} &= \int_{x_f}^{x_{\text{hbend}}} A_{\text{hbend}(x)}\, dx \\
&= A_2 \frac{1}{3}\left[(x_{\text{shell}_2} - x_f)^3 - (x_{\text{shell}_2} - x_{\text{hbend}})^3\right] \\
&+ A_1 \frac{1}{2}\left[(x_{\text{tail}} - x_f)^2 - (x_{\text{tail}} - x_{\text{hbend}})^2\right] \\
&+ A_0 (x_{\text{hbend}} - x_f) && \text{(A.95)} \\
\mathcal{V}_{\text{hbend}_b} &= \int_{x_b}^{x_{\text{hbend}}} A_{\text{hbend}(x)}\, dx \\
&= A_2 \frac{1}{3}\left[(x_{\text{shell}_2} - x_b)^3 - (x_{\text{shell}_2} - x_{\text{hbend}})^3\right] \\
&+ A_1 \frac{1}{2}\left[(x_{\text{tail}} - x_b)^2 - (x_{\text{tail}} - x_{\text{hbend}})^2\right] \\
&+ A_0 (x_{\text{hbend}} - x_b) && \text{(A.96)} \\
\mathcal{V}_{\text{hbend}_c} &= \frac{1}{2}\left[A_{\text{hbend}(x_b)} + A_{\text{hbend}(x_f)}\right] c_o \bar{w} && \text{(A.97)} \\
\mathcal{V}_{\text{hbend}} &= \mathcal{V}_{\text{hbend}_f} + \mathcal{V}_{\text{hbend}_c} + \mathcal{V}_{\text{hbend}_b} && \text{(A.98)} \\
W_{\text{hbend}} &= \rho_{\text{bend}}\, g\, \mathcal{V}_{\text{hbend}} && \text{(A.99)} \\
x W_{\text{hbend}} &= x_{\text{wing}} W_{\text{hbend}} && \text{(A.100)}
\end{aligned}
$$

**Added vertical-axis bending material**

The vertical-axis bending moment on the rear fuselage is entirely due to the airload on the vertical tail (A.75), reduced by the $r_{\text{Mv}}$ factor to account for inertial relief.

$$
\mathcal{M}_{\text{v}(x)} = r_{\text{Mv}}\, L_{\text{v}_{\text{max}}} (x_{\text{tail}} - x) \qquad \text{(A.101)}
$$

Since the wing is assumed to react the local $\mathcal{M}_{\text{v}}$ via its large yaw inertia, as sketched in Figure A.5, the moment distribution (A.101) is imposed only on the rear fuselage. The required bending inertia $I_{\text{vbend}(x)}$ and area $A_{\text{vbend}(x)}$ are then sized to keep the axial stress constant. The defining relations follow the ones for the horizontal-axis case above.

$$
E_{\text{bend}} \epsilon_{x(x)} = r_E \left( \frac{\mathcal{M}_{\text{v}(x)}\, w_{\text{fuse}}}{I_{\text{vshell}} + r_E\, I_{\text{vbend}(x)}} + \frac{\Delta p}{2} \frac{R_{\text{fuse}}}{t_{\text{shell}}} \right) \le \sigma_{\text{bend}} \qquad \text{(A.102)}
$$

$$
\text{where} \qquad w_{\text{fuse}} = R_{\text{fuse}} + w_{\text{db}} \qquad \text{(A.103)}
$$

$$
I_{\text{vbend}(x)} = \max\left( \frac{\mathcal{M}_{\text{v}(x)}\, w_{\text{fuse}}}{\sigma_{\text{Mv}}} - \frac{I_{\text{vshell}}}{r_E} \;,\; 0 \right) \qquad \text{(A.104)}
$$

$$
\text{where} \qquad \sigma_{\text{Mv}} = \sigma_{\text{bend}} - r_E \frac{\Delta p}{2} \frac{R_{\text{fuse}}}{t_{\text{shell}}} \qquad \text{(A.105)}
$$

$$
A_{\text{vbend}(x)} = \frac{I_{\text{vbend}(x)}}{w_{\text{fuse}}^2} = B_1 (x_{\text{tail}} - x) + B_0 \qquad \text{(A.106)}
$$

$$
\text{where} \qquad B_1 = \frac{r_{\text{Mv}} L_{\text{v}}}{w_{\text{fuse}}\, \sigma_{\text{Mv}}} \qquad \text{(A.107)}
$$

$$B_0 \;=\; -\frac{I_{\text{vshell}}}{r_E\, w_{\text{fuse}}^2} \tag{A.108}$$

The volume and weight of the added bending material is defined by integration of $A_{\text{vbend}(x)}$ over the rear fuselage, from the rear of the wing box $x_b$, up to the point $x = x_{\text{vbend}}$ where $A_{\text{vbend}} = 0$ in definition (A.106).

$$\begin{aligned}
\mathcal{V}_{\text{vbend}_b} &= \int_{x_b}^{x_{\text{vbend}}} A_{\text{vbend}(x)}\, dx \\
&= B_1 \frac{1}{2}\left[(x_{\text{tail}} - x_b)^2 - (x_{\text{tail}} - x_{\text{vbend}})^2\right] \;+\; B_0\,(x_{\text{vbend}} - x_b) && \text{(A.109)} \\
\mathcal{V}_{\text{vbend}_c} &= \frac{1}{2} A_{\text{vbend}(x_b)}\, c_o \bar{w} && \text{(A.110)} \\
\mathcal{V}_{\text{vbend}} &= \mathcal{V}_{\text{vbend}_c} \;+\; \mathcal{V}_{\text{vbend}_b} && \text{(A.111)} \\
W_{\text{vbend}} &= \rho_{\text{bend}}\, g \mathcal{V}_{\text{vbend}} && \text{(A.112)} \\
x\!W_{\text{vbend}} &= \tfrac{1}{3}(2x_{\text{wing}} + x_{\text{vbend}}) W_{\text{vbend}} && \text{(A.113)}
\end{aligned}$$

For simplicity, the $W_{\text{hbend}}, W_{\text{vbend}}$ weights' contributions to $\mathcal{M}_{\text{h}}$ are excluded from (A.79) and the subsequent calculations. A practical reason is that the added material does not have a simple distribution, and hence would greatly complicate the $\mathcal{M}_{\text{h}(x)}$ function, thus preventing the analytic integration of the added material's weight. Fortunately, the added bending material is localized close to the wing centroid and hence its contribution to the overall bending moment is very small in any case, so neglecting its weight on the loading is well justified at this level of approximation.

### A.2.4 Total Fuselage Weight

The total fuselage weight includes the shell with stiffeners, tailcone, floor beams, fixed weight, payload-proportional equipment and material, seats, and the added horizontal and vertical-axis bending material.

$$\begin{aligned}
W_{\text{fuse}} &= W_{\text{fix}} \;+\; W_{\text{apu}} \;+\; W_{\text{padd}} \;+\; W_{\text{seat}} \\
&\quad + W_{\text{shell}} \;+\; W_{\text{cone}} \;+\; W_{\text{window}} \;+\; W_{\text{insul}} \;+\; W_{\text{floor}} \\
&\quad + W_{\text{hbend}} \;+\; W_{\text{vbend}} && \text{(A.114)} \\
x\!W_{\text{fuse}} &= x\!W_{\text{fix}} + x\!W_{\text{apu}} + x\!W_{\text{padd}} + x\!W_{\text{seat}} \\
&\quad + x\!W_{\text{shell}} + x\!W_{\text{cone}} + x\!W_{\text{window}} + x\!W_{\text{insul}} + x\!W_{\text{floor}} \\
&\quad + x\!W_{\text{hbend}} + x\!W_{\text{vbend}} && \text{(A.115)}
\end{aligned}$$

### A.2.5 Wing or Tail Planform

The surface geometry relations derived below correspond to the wing. Most of these apply equally to the tails if the wing parameters are simply replaced with the tail counterparts. The exceptions which pertail to only the wing will be indicated with "(Wing only)" in the subsection title.

### Chord distribution

The wing or tail surface is assumed to have a two-piece linear planform with constant sweep $\Lambda$, shown in Figure A.6. The inner and outer surface planforms are defined in terms of the center chord $c_o$ and the inner and outer taper ratios.

$$\lambda_s = c_s/c_o \tag{A.116}$$
$$\lambda_t = c_t/c_o \tag{A.117}$$

Similarly, the spanwise dimensions are defined in terms of the span $b$ and the normalized spanwise coordinate $\eta$.

$$\eta = 2y/b \tag{A.118}$$
$$\eta_o = b_o/b \tag{A.119}$$
$$\eta_s = b_s/b \tag{A.120}$$

For generality, the wing center box width $b_o$ is assumed to be different from the fuselage width to allow possibly strongly non-circular fuselage cross-sections. It will also be different for the tail surfaces. A planform break inner span $b_s$ is defined, where possibly also a strut or engine is attached. Setting $b_s = b_o$ and $c_s = c_o$ will recover a single-taper surface.

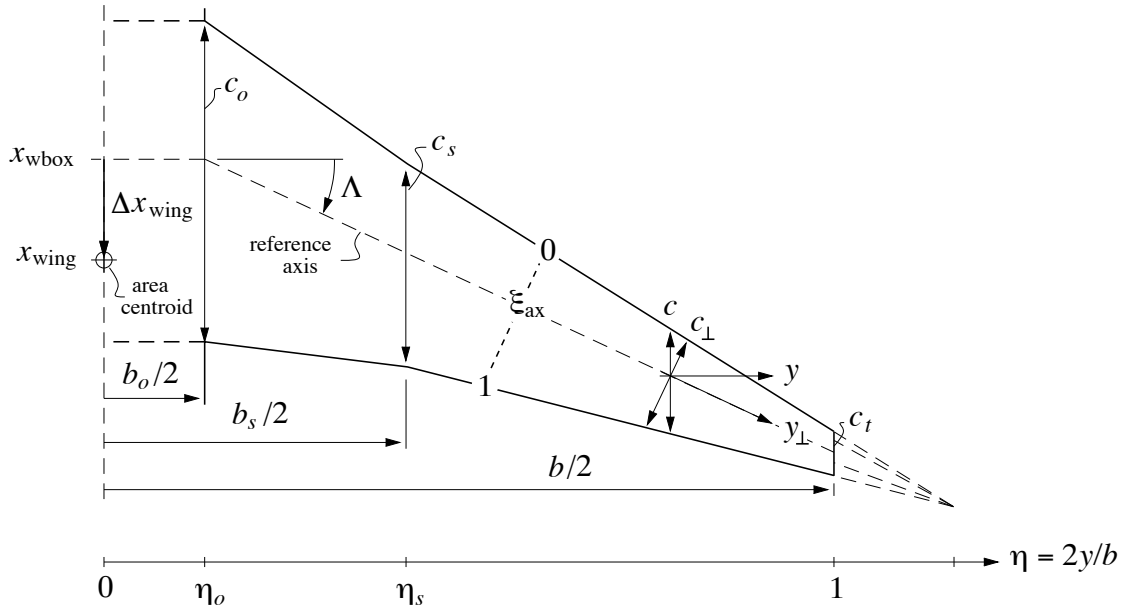


Figure A.6: Piecewise-linear wing or tail surface planform, with break at $\eta_s$.

It's convenient to define the piecewise-linear normalized chord function $C_{(\eta)}$.

$$\frac{c_{(\eta)}}{c_o} \equiv C_{(\eta;\eta_o,\eta_s,\lambda_s,\lambda_t)} = \begin{cases} 1 & , \quad 0 < \eta < \eta_o \\ 1 + (\lambda_s - 1)\dfrac{\eta-\eta_o}{\eta_s-\eta_o} & , \quad \eta_o < \eta < \eta_s \\ \lambda_s + (\lambda_t - \lambda_s)\dfrac{\eta-\eta_s}{1-\eta_s} & , \quad \eta_s < \eta < 1 \end{cases} \tag{A.121}$$